frontiers | Frontiers in Earth Science

ORIGINAL RESEARCH
published: 16 May 2022
doi: 10.3389/feart.2022.876913

Gas Hydrate Dissociation Events During LGM and Their Potential Trigger of Submarine Landslides: Foraminifera and Geochemical Records From Two Cores in the Northern South China Sea

Yi Huang[1,2], *Jun Cheng*[1,2,3], *Mingmin Wang*[1,2,3], *Shuhong Wang*[1,2]* *and Wen Yan*[1,2,3]

[1]*Southern Marine Science and Engineering Guangdong Laboratory (Guangzhou), Guangzhou, China,* [2]*Key Laboratory of Ocean and Marginal Sea Geology, South China Sea Institute of Oceanology, Chinese Academy of Sciences, Guangzhou, China,* [3]*University of Chinese Academic of Sciences, Beijing, China*

OPEN ACCESS

Edited by:
Lihua Zuo,
Texas A&M University Kingsville, United States

Reviewed by:
Luigi Jovane,
University of São Paulo, Brazil
Xianrong Zhang,
Qingdao Institute of Marine Geology (QIMG), China

***Correspondence:**
Shuhong Wang
wshds@scsio.ac.cn

Specialty section:
This article was submitted to Marine Geoscience, a section of the journal Frontiers in Earth Science

Received: *16 February 2022*
Accepted: *28 April 2022*
Published: *16 May 2022*

Citation:
Huang Y, Cheng J, Wang M, Wang S and Yan W (2022) Gas Hydrate Dissociation Events During LGM and Their Potential Trigger of Submarine Landslides: Foraminifera and Geochemical Records From Two Cores in the Northern South China Sea. Front. Earth Sci. 10:876913. doi: 10.3389/feart.2022.876913

Although submarine slope failures and occurrence of gas hydrates are well known in the Dongsha area of the South China Sea the potential relationship between the aforementioned phenomena has not been clearly understood yet. Herein, we present carbon and oxygen isotope compositions of benthic foraminifera and sulfur isotopic composition of chromium reducible sulfur (CRS; $\delta^{34}S_{CRS}$) from two cores from the Dongsha slope, aiming at identifying gas hydrate dissociation events in geological history. The geochemical data indicated that a large amount of gas hydrate dissociated at the beginning of the Last Glacial Maximum (LGM). Meanwhile, disturbances in the sedimentary strata revealed that a submarine landslide occurred at the end of the Last Glacial Maximum. Moreover, the associated abrupt increase of benthic foraminifera abundance implies that the submarine landslide was probably caused by an intense methane releasing from gas hydrate dissociation. A smaller scale submarine landslide related to gas hydrate dissociation was also recorded in core 973-5, retrieved from the flat area at the base of the slope.

Keywords: gas hydrate, submarine landslide, benthic foraminifera, Dongsha area, South China Sea

INTRODUCTION

It is known that methane-rich fluids due to subsurface gas hydrate dissociation leak to the seafloor at specific sites on continental slopes the world over (Boetius and Wenzhoefer, 2013). In these systems, usually most of the methane and higher hydrocarbons are consumed by anaerobic oxidation of methane (AOM) coupled with sulfate reduction in the uppermost sedimentary layers (Boetius et al., 2000; Boetius and Wenzhoefer, 2013). This process leads to geochemical anomalies in the shallow surface sediment and porewater, favoring the precipitation of authigenic carbonates in the sulfate-methane transition zone (SMTZ) (Boetius and Wenzhoefer, 2013). Thus, AOM signals can be recorded by geochemical anomalies in authigenic carbonates, such as extremely negative $\delta^{13}C$ values (Roberts and Aharon, 1994; Peckmann and Thiel, 2004; Pierre et al., 2016). Authigenic carbonates are good archives to study methane seepage, but because of it is not continuous when precipating and

TABLE 1 | The location and length of the sample cores.

Core name	Longitude (E)	Latitude(N)	Water depth(m)	Length(m)
973-4	118°49.0818′	21°54.3247′	1,666	13.75
973-5	119°11.0066′	21°18.5586′	2,998	9.25

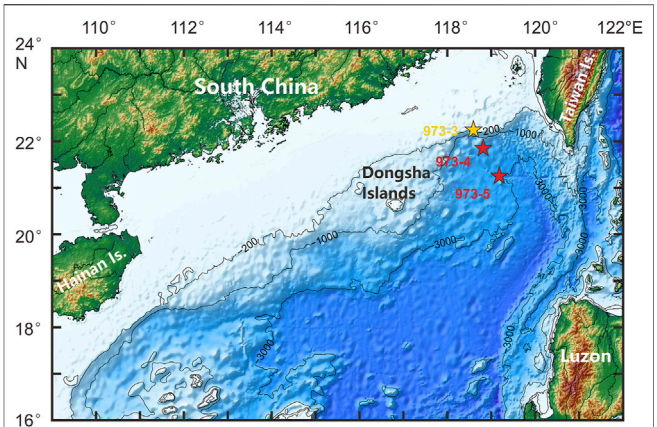

FIGURE 1 | Sampling stations in the Dongsha area of the northern SCS. Red stars represent the two sampling cores 973-4 and 973-5, and the yellow star represents the core 973-3 (Chen et al., 2014).

sometimes difficult to get proper samples, it is hard to reveal the evolution of the whole process of methane seepage. In contrast, sediment cores can serve as a potential archive to reconstruct the evolution of past methane seepage, especially when combined with age data (Bayon et al., 2015; Li et al., 2018). Specifically, $\delta^{34}S_{CRS}$ of sediments and $\delta^{13}C$ of foraminifera are the most commonly used research object in sediment cores. The $\delta^{34}S_{CRS}$ in the sediments is confirmed to be heavier in the SMTZ where the sulfate concentrations in the pore water has a rapid decrease, and consequently this value can be used to recognize paleo-SMTZs in the geological record (Peketi et al., 2012; Borowski et al., 2013; Gong et al., 2018). Benthic foraminifera near cold seep areas generally occur in large quantities, with wide areal distributions, short life cycles and stable shell preservation in the sediments after death. Thus, they are excellent for recording the effects of gas hydrate dissociation (Rathburn et al., 2000; Portilho-Ramos et al., 2018). Benthic foraminifera associations (Panieri, 2005) and the stable isotope composition of specific benthic foraminifera can therefore be used to record methane seepage activity in the geological record (Wefer et al., 1994; Stott et al., 2002; Herguera et al., 2014; Schneider et al., 2018). Although the fact that epigenetic carbonate precipitation plays a dominant role in the distinctly negative $\delta^{13}C$ record of benthic foraminifera is still controversial (Consolaro et al., 2015; Panieri et al., 2017), it is opportune to mention that the microstructure and geochemical characteristics of foraminifera influenced by post diagenesis can also trace the methane emissions in a geological period (Schneider et al., 2017). So AOM signals in cold seep environments are recorded in the foraminifera shells. It is well known that hydrate dissociation are likely to trigger intensive methane seepage (Chen et al., 2016), resulting in an abnormally high pore pressure and a reduction in the effective stress of continental slope sediments. When the amount of gas emission is massive enough or the continental slope with gas hydrate is steep, the fluidized decomposition zone will form a downward sliding surface. In this situation, any small perturbation of the stress, such as an earthquake, or the self-gravity of the sediments, may lead to slope failure (Kayen and Lee, 1991). Many submarine landslides are proved to be related to gas hydrate dissociation in the world, including the Storegga slide, off the coast of Norway, and Cape Fear, on the Atlantic continental slope (Leynaud et al., 2004; Solheim et al., 2005; Chaytor et al., 2009; Horozal et al., 2017). In the geological history, there are also some numerical simulation and sedimentary records that demonstrate the rapid changes of sedimentation affect the gas seepage activity, which also indicates the spatial and temporal charateristics of methane seepage (Karstens et al., 2018; Screaton et al., 2019). However, other researches argue that the destabilization of a hydrate system is a slow process and could be largely delayed by overpressure accumulation (Colin et al., 2020). Recently, climate-driven increase in temperature, especially during last deglacial (MIS5e), is proved to be a trigger factor of gas hydrate dissociation in SCS (Chen et al., 2019). Thus, the questions concerning the main cause of gas hydrate dissociation are still under debate, the subsequently methane seepage and its potential link to the submarine landslides are poorly documented. Many studies have identified the occurrence of fluidized decomposition zone by geophysical methods, such as seisetic reflection data (Eiger et al., 2017; Handwerger et al., 2017), little attention has been paid to the geochemical characteristics of gas hydrate and landslide deposits. The Dongsha area, which is located on the continental slope of the northeastern South China Sea (SCS), is an excellent area for such a study. The extensive development of gas chimneys, submarine landslides, mud diapirs, carbonate mounds and active cold seeps in this area (Chen et al., 2005; Yan et al., 2006; Yu et al., 2013; Feng and Chen, 2015; Wu et al., 2018), strongly suggests the occurrence of gas hydrate reservoirs (Chen et al., 2005; Li et al., 2011; Su et al., 2012). Here, by using the carbon-sulfate-benthic foraminifera system, two sediment cores in Dongsha slope are used to identify gas hydrate dissociation events and discuss the causal relationship between gas emissions and submarine landslides.

MATERIALS AND METHODS

Sediment cores 973-4 and 973-5 were collected from the middle of the slope and the flat area at the base of the Dongsha area, in the northern SCS, respectively, using a piston corer during the 973 cruise by the ship "R/V OceanVI" in 2011 (**Table 1**; **Figure 1**).

The core 973-4 is mostly made of grey and grey-green clay, with coarser-grain-size silt at the depth of 450–600 cm, in which foraminifera is abundant. Below 600 cm, there are black hydrogen sulfide disseminated plaque deposits with a distinct smell of rotten eggs. For the core 973-5, it is also mostly made of grey to grey-dark clay, the obvious foraminifera enriched silt layer occurred at around 250 ~300 cm there is an angular

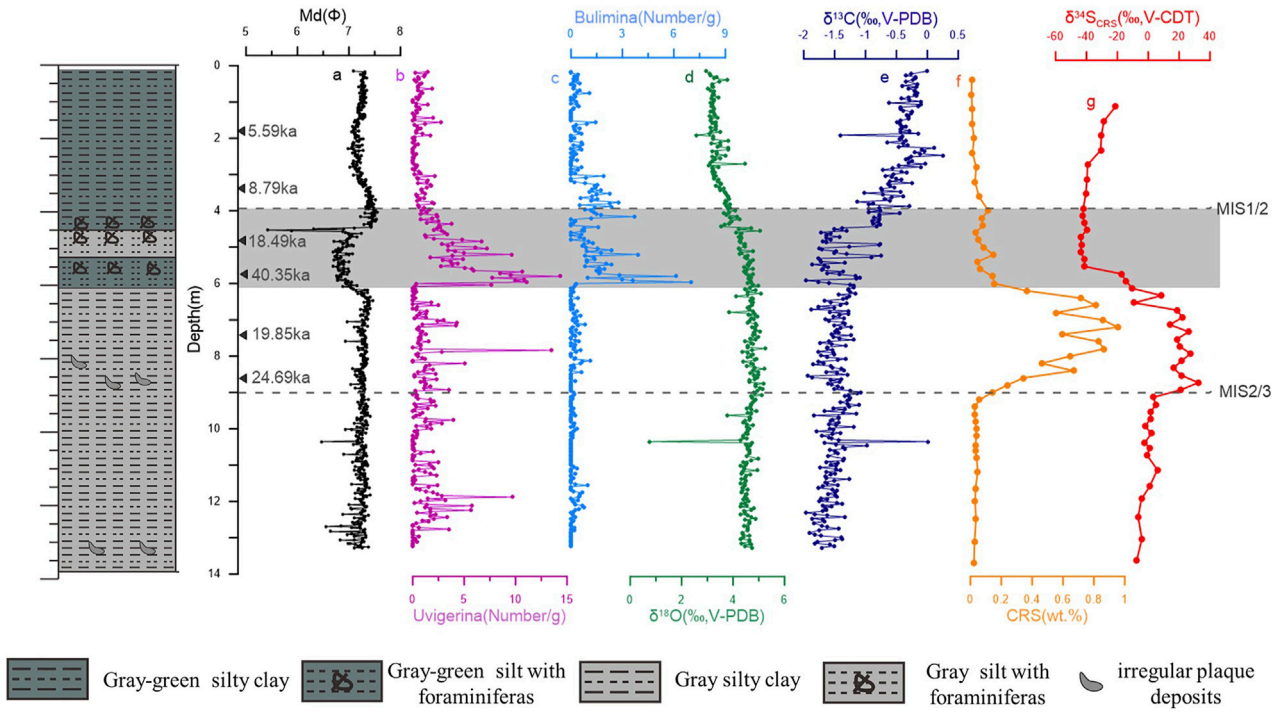

FIGURE 2 | Sediment particle size and geochemical records of core 973-4, lithostratigraphic picture (left) **(A)** Medium size, **(B)** quantity of *Uvigerina* spp., **(C)** quantity of *Bulimina* spp., **(D)** oxygen isotopes of *Uvigerina* spp., **(E)** carbon isotopes of *Uvigerina* spp., **(F)** CRS, **(G)** sulfur isotopic compositions. The triangles indicate the AMS^{14}C dating results (Zhang et al., 2018); the dashed lines indicate the demarcation lines of MIS1/MIS2 and MIS2/MIS3; and the shadowed horizon indicates horizons influenced by submarine landslides.

unconformity at around 460 cm. Sediment samples were collected every 2 cm from 15 cm bsf (below the seafloor) to the core bottom, except in the top 15 cm of each core, where only one sample was collected. Grain size measurements were carried out at the South China Sea Institution of Oceanology, Chinese Academic of Sciences, using a Mastersizer2000 Laser Particle Size Analyzer. The particle classification was 1Φ [Φ = $-\log_2 d$; d means particle diameter (mm)]. The detection limit was between 0.5 and 2000 μm, and the relative error was less than 3%. The benthic foraminifera *Uvigerina* spp. and *Bulimina* spp. were picked from the >200 μm-size fractions to calculate the assemblage density (number of individuals per gram of dry sediment) and perform the isotopic analysis (*Uvigerina* spp.). The $\delta^{13}C$ and $\delta^{18}O$ isotopes of foraminifera tests were measured on aMAT253 Stable Isotope Gas Mass Spectrometer in the South China Sea Institution of Oceanology, Chinese Academic of Sciences and calibrated to the VPDB standard. Analytical precision was estimated to be better than 0.03‰ for $\delta^{13}C$ and 0.08‰ for $\delta^{18}O$. CRS (chromium reducible sulfur, mainly FeS, FeS_2) in the bulk sediments were extracted following the method of Canfield (Canfield et al., 1986). two to five gcarbonate powder was digested in 6 mol/L HCl at 50°C for 6 h to release acid volatile sulfur under a continuous flow of N2 (g) and the residue (remain mainly as FeS and FeS_2) was analyzed for bulk carbonate CRS. CRS was extracted using 6 N HCl and 1M $CrCl_2$ for 3 h in 100% N2 atmosphere. The H2S evolved was driven via N2 carrier into 0.1 N $AgNO_3$ and trapped as Ag_2S for gravimetric and then isotopic measurements (Gong et al., 2018). The sulfur isotope analysis was performed at the Louisiana State University, using an Elemental Analyzer (EA) at 980°C, and subsequently with a Thermo-Electron Delta V Plus Advantage mass spectrometer. The standard deviation associated with $\delta^{34}S$ analysis was ±0.3‰, and reported relative to the VCDT (Vienna Canyon Diablo Troilite) standard.

RESULTS

Median Particle Size

Median particle size is commonly used to represent the average particle size of sediments (Hu et al., 2017; Li et al., 2018). The sediments in core 973-4 were fine-grained in most layers, but the grain size in the 4.3–6.0 m layer was significantly coarser (**Figure 2**). Core 973-5 contained fine-grained sediment in most layers, without any significant differences in the particle size being observed throughout the core; only a minor increase in coarser content was found in several layers (e.g., 1.3–2.7 m, 3.9–4.0 m, 5.9–6.0 m, 8.2–8.4 m, **Figure 3**).

Foraminifera Content

The foraminifera-rich layer (4.3–6.0 m) in core 973-4 is consistent with the high content of the sediment coarse fraction (**Figures 2B,C**). The numbers of the two species were almost always less than five per gram below 6 m bsf. This number

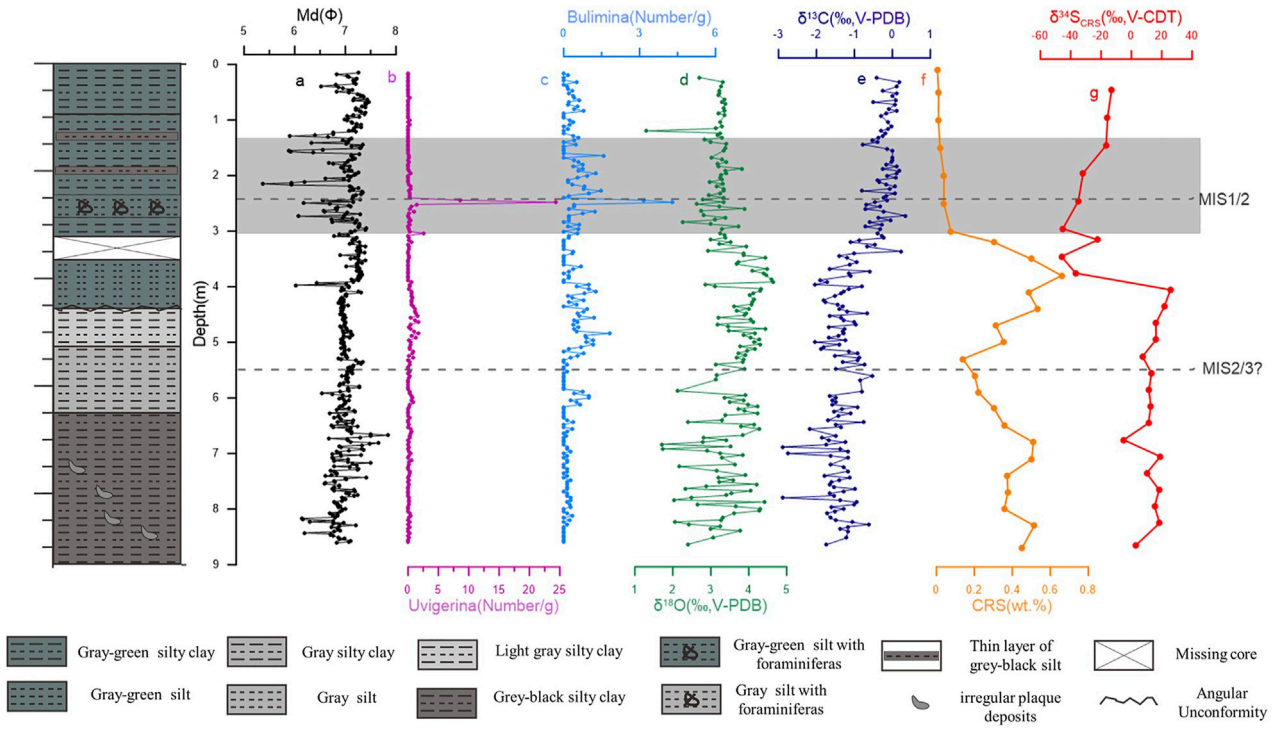

FIGURE 3 | Sediment particle size and geochemical records of core 973-5,lithostratigraphic picture (left) **(A)** Medium size, **(B)** quantity of *Uvigerina* spp., **(C)** quantity of *Bulimina* spp., **(D)** oxygen isotopes of *Uvigerina* spp., **(E)** carbon isotopes of *Uvigerina* spp., **(F)** CRS, **(G)** sulfur isotopic compositions, triangles indicate the AMS ^{14}C dating results (Wang, 2013); the dashed lines indicate the demarcation lines of MIS1/MIS2 and MIS2/MIS3; and the shadowed horizon indicates horizons influenced by submarine landslides.

increases abruptly to more than 10 per gram at about 6 m bsf and then gradually decreases upward until 4.3 mbsf. Low values are observed in the uppermost 4.3 m bsf of the core (**Figures 2B,C**). In core 973-5, the numbers of benthic foraminifera were far less than core in 973-4 and few foraminifera were seen in the whole core, except in a few layers (e.g., at depths of about 2.5 m, 4.0–5.5, and 6 m; **Figures 3B,C**).

Carbon and Oxygen Isotope Compositions of Uvigerina

The δ^{18}O composition of Uvigerina spp. in the core 973-4 varied from 2.57 to 5.26‰, with lighter δ^{18}O values in the upper part of the core (**Figure 2D**). The δ18O depletion fits well with the Deglaciation transition layer at about 4.3 m bsf and shows stable values in the uppermost core. In core 973-5, δ^{18}O values show a broad range of variation below 5.5 m bsf (**Figure 3D**), and values between 2.93 and 4.49‰ at the 3.3–3.6 m bsf layer, corresponding to the deglaciation transition. The δ^{13}C values for Uvigerina spp. in core 973-4 ranged from −1.97 to 0.25‰ with an average value of −1.15‰ (**Figure 2E**). The δ^{13}C values below 4.3 m bsf are obviously negative, with only small fluctuations; above this depth they become heavier until the surface. In core 973-5, the δ13C values were consistently negative below the depth of 3.3 m bsf and showed heavier trend from -2.9 to 0.18‰ in the upper part of the core (**Figure 3E**).

CRS and δ^{34}SCRS Values

In core 973-4, the CRS contents vary between 0.01 wt‰ and 0.95 wt‰. A high CRS content was observed in the interval 6.8–9.0 m (**Figure 2G**). The δ^{34}SCRS values show a wide variation, ranging from −43.8 to 32.6‰. The sulfate isotope compositions show extremely positive values at the CRS enrichment depth (6.8–9.0 m), and then are lower elsewhere, with a minimum value of −43.8‰ in the interval 2.8–5.6 m (**Figure 2F**). In core 973-5, high CRS contents and positive $\delta^{34}S_{CRS}$ values are observed below 4 m bsf (**Figure 3G**), and the $\delta^{34}S_{CRS}$ values above this depth become lighter, ranging from -46‰ to -15.7‰ (**Figure 3F**).

DISCUSSION

Radiocarbon- and δ^{18}O-derived age models (Zhang et al., 2018) suggested that two studied cores, 973-4 and 973-5, recorded sediment deposition since MIS3. Combined with the oxygen isotope change curve and previous research (Liu et al., 2018), we found that the 4.0–9.0 m bsf layer in core 973-4 records the sediment of MIS2, and the layer above 4.0 m corresponds to the sediment deposited since the Holocene. Interestingly, there was an age inversion around 5.8 m (40.35ka). The strata of MIS3 may be disturbed and MIS3 sediments have been reversed to MIS2. The age inversion intervals coincide with the foraminifera-rich

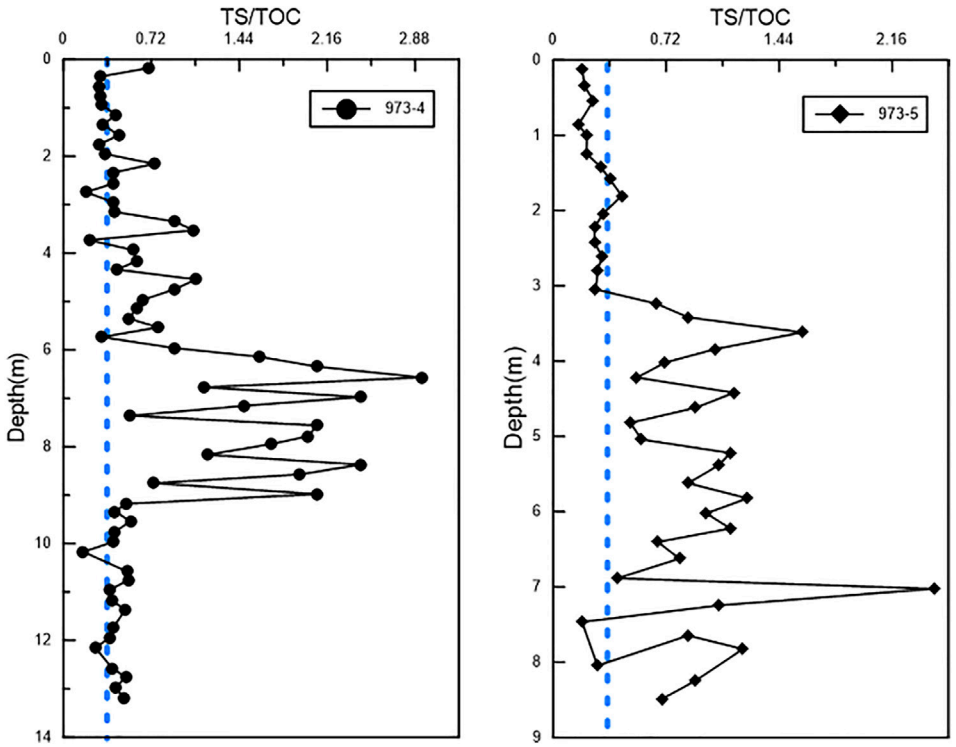

FIGURE 4 | TS/TOC ratios in the cores 973-4 and 973-5 (TS and TOC data cited from (Zhang et al., 2018); the blue dashed lines indicate the S/C ratio in normal marine sediment).

and sand content-rich layers (4.4–6.0 m), and possibly resulted from landslides or physical disturbance by intense seepage (Lin et al., 2016). In core 973-5, the demarcation lines of MIS1/2 and MIS2/3 are at the depths of 2.2 and 4.8 m bsf respectively; the age absence in 4.8 m bsf may also have been caused by a landslide.

Geochemical Records of Gas Hydrate Dissociation Events

In the typically anoxic subseafloor marine sediments, the consumption of porewater sulfate is controlled by two microbially mediated processes: 1) organo clastic sulfate reduction (OSR) (Berner, 1982); and 2) anaerobic oxidation of methane (AOM) (Boetius et al., 2000). The two net reactions are expressed stoichiometrically as follows: $2CH_2O + SO_4^{2-} \rightarrow 2HCO_3^- + H_2S$ 1) $CH_4 + SO_4^{2-} \rightarrow HCO_3^- + HS^- + H_2O$ 2) However, these two different processes always result in different average S/C ratio in sediments. In oxic and suboxic marine sediments (OSR dominate), the reduced sulfur and total organic carbon (TOC) contents typically show a positive correlation with an average S/C ratio of 0.36 (Berner, 1982). In our studied cores, the TOC content was typically low (Zhang et al., 2018), and the S/C ratios at 6.0–9.0 m bsf (973-4) and below 4.0 m bsf (973-5) were higher than 0.36 (**Figure 4**). These situations were referred to an organically-limited and methane-rich environment, in which AOM was the dominant process, contributed to a significant fraction of sulfides (Kaneko et al., 2010; Lim et al., 2011; Sato et al., 2012) and may have significantly increased the S/C ratios of sediments. This AOM origin for sulfides explains why there was no correlations between the CRS and TOC contents in the sediments of both cores (**Figure 5**).

Positive $\delta^{34}S$ (up to 32.6‰) values of sulfide minerals could represent a present- or paleo-SMTZ (sulfate-methane transition zone) where AOM process occurred strongly (Aharon and Fu, 2003; Jorgensen et al., 2004; Borowski et al., 2013; Zhu et al., 2013). In the studied cores, the $\delta^{34}S_{CRS}$ values below 6.0 m bsf in core 973-4 and below 4.0 m bsf in the core 973-5 are positive. Especially in the 6.0–9.0 m bsf layer of core 973-4, a wide SMTZ with positive sulfur isotope compositions up to 20‰ represents a sustained and stable methane flux. As shown in the **Figure 2G**, at the end of the LGM period (4.0–6.0 m) with a low sea-level stage, the $\delta^{34}S_{CRS}$ became highly negative (−43.8‰ to −39.4‰). The low $\delta^{34}S$ values in seep-impacted sediments may be attributed to iron limitation caused by low sedimentation rates (Formolo and Lyons, 2013) or disproportionation of microbial sulfur occurring close to the sediment-water interface (Canfield and Thamdrup, 1994; Borowski et al., 2013). Because the sedimentation rate of our study area is typically high at low sea level stands (Zhang et al., 2018), disproportionation of microbial sulfur instead of iron limitation might be the reason for the low $\delta^{34}S_{CRS}$ values.

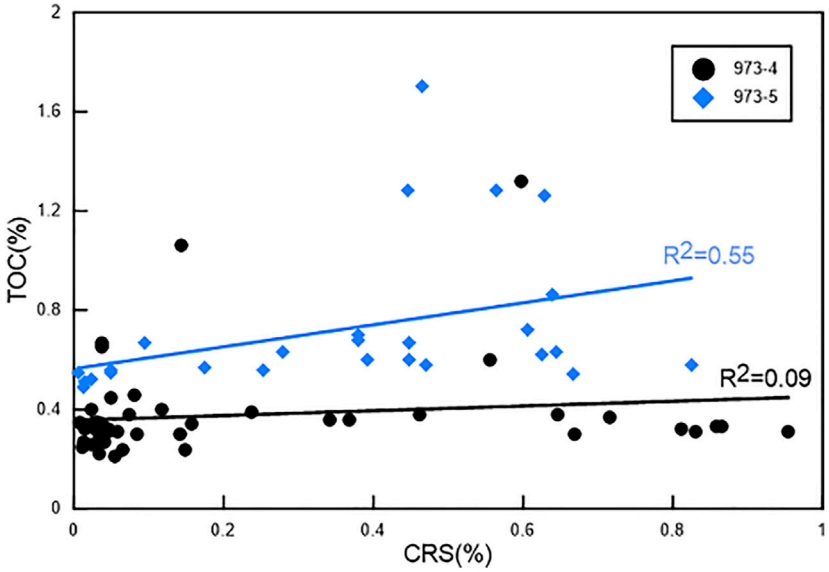

FIGURE 5 | The correlations between TOC and CRS in cores 973-4 and 973-5 (Zhang et al., 2018).

Generally, disproportionation of microbial sulfur happen in an open system, which can be caused by intense methane flux (Li et al., 2018). Herein, we suppose the low $\delta^{34}S$ values might be also caused by this phenomenon in this period.

Response of Specific Benthic Foraminifera to Gas Hydrate Dissociation Events

According to previous research, the $\delta^{13}C$ values of *Uvigerina* spp. in normal seawater range from −0.1 to 1.0‰ (Rathburn et al., 2003; Schmiedl et al., 2004; Fontanier et al., 2006). However, in our studied cores, the $\delta^{13}C$ values of benthic foraminifera below 3.9 m bsf in core 973-4 and 2.5 m bsf in core 973-5 (corresponding to the end of the Last Glacial period) were almost all lower than -1.0‰, showing an obvious negative carbon bias. Although some researchers considered that the $\delta^{13}C$ values in the Glacial period were more negative than that in Deglacial period (Wei et al., 2006), the $\delta^{13}C$ values of benthic foraminifera in the northern SCS always vary from about -0.6 to 0.2‰ (range variation of approximately 0.8‰ in the past 90 ka) under the influence of climate change (Wei et al., 2006). These indicate that such wide range of the carbon negative bias (e.g.,1.9‰ in core 973-4) in our study area was not caused by climate change and seem to be caused by AOM reaction. In addition, when recording methane seepage activity, a wide range of $\delta^{13}C$ values of benthic foraminifera are more appropriate than absolute negative values (Rathburn et al., 2003). Thus, the carbon negative bias can be attributed to methane seepage in the studied cores. Because ^{18}O is higher in cold seep fluids, and the heavier $\delta^{18}O$ values were thought to be another evident of gas hydrate dissociation or cold seep activity (Uchida et al., 2004). In core 973-4 and 973-5, the $\delta^{18}O$ values were obviously heavier during the Glacial period in both cores, which is consistent with the $\delta^{13}C$ results. Thus we can tentatively deduce the methane seepage activities in the core 973-4 by analyzing the $\delta^{13}C$ and $\delta^{18}O$ values change. **Figure 2E** shows negative carbon isotope compositions in MIS2 (4.0–9.0 m), indicating a sustained methane seepage during this period. Furthermore, other reports have suggested that cold seeps were particularly active at low sea-level stands due to a hydrostatic pressure reduction in the SCS (Tong et al., 2013; Han et al., 2014), hence it supports our hypothesis that an intense methane seepage happened during LGM (4.0–6.0 m). Since the end of the LGM (above 4.0 m), the $\delta^{13}C$ values in core 973-4 were quite stable and comparable to normal sea-water values typical of non-seep environments. This implies that the gas hydrate dissociation events gradually weakened in this core since the Holocene. As the temperature rose gradually in the Deglaciation periods, the changes in global ice volume and bottom water temperature were not the dominant factors for hydrate decomposition. Instead, as the sea level and the hydrostatic pressure on the sediment have gradually increased since the Last Glacial, the gas hydrate stability zone has thickened, thus causing a weakening of gas hydrate dissociation and methane seepage. *Uvigerina* spp. and *Bulimina* spp. are considered as specific endophytic benthic foraminifera that can adapt to the modern cold seep environments with high TOC and low oxygen content (Abu-Zied et al., 2008), and they were the two dominant species of benthic foraminifera in cores 973-4 and 973-5. Moreover, as shown in **Figures 2B,C**, their numbers increased to different extents during the Last Glacial period (4.0–9.0 m of core 973-4), which may be under the influence of the methane flux related to the gas hydrate dissociation during that time (Chen et al., 2007). However, previous research indicated that normal cold seep activity cannot significantly change the total abundance of benthic foraminifera (Panieri et al., 2009). Therefore, the large increases in the number of benthic foraminifera at the end of the LGM period (4.0–6.0 m of core 973-4), especially the abrupt increase in the layer

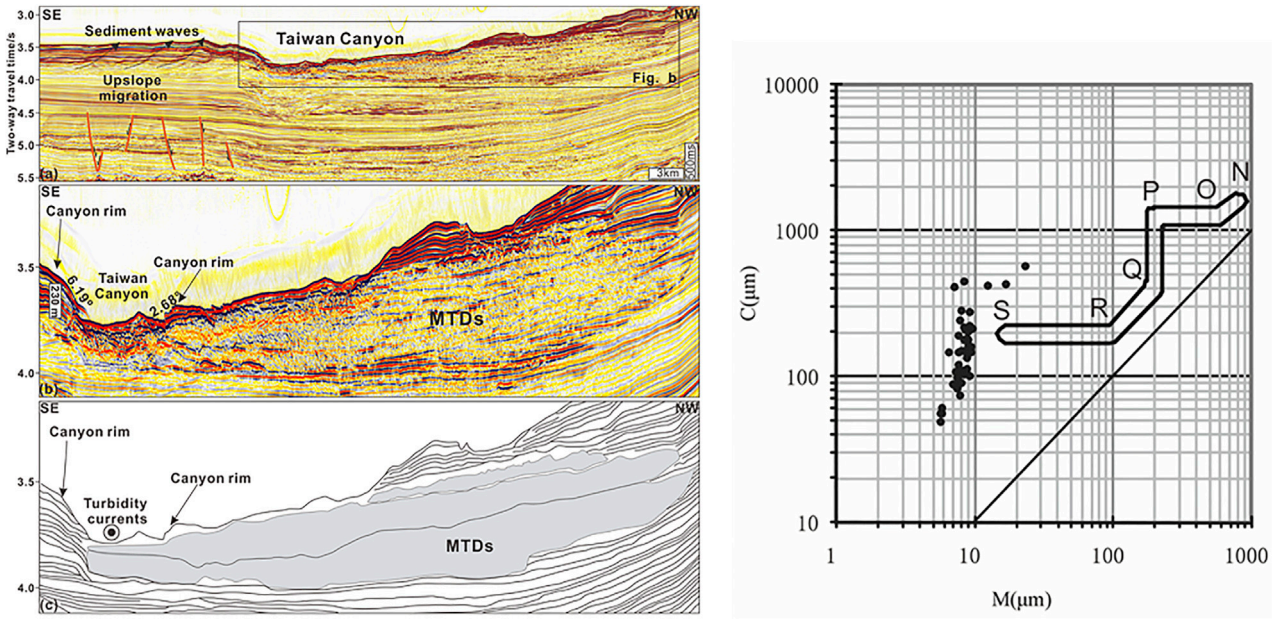

FIGURE 6 | The seismic profile of the D2 survey line (from Li, 2020, left) and Passega C-M diagram (Passega, 1964, right). C = maximum (D99; first percentile) grain size of 973-4, M = median grain size. The dots represent the interval (4–6 m) with coarser grain content. **(A)** Two-dimensional (2D) seismic profile of the Taiwan Canyon highlighting the morphological differences in canyon banks. **(B)** The mass transport deposits (MTDs) are characterized by chaotic amplitude reflections. **(C)** Line drawn interpretation of **(B)** illustrating the presence of widespread MTDs in the north-east of Taiwan Canyon.

at about 6 m bsf in core 973-4, is more likely associated with geological events rather than to large quantities of methane fluid. Sustained methane seepage can provide a rich food source for benthic foraminifera (Schonfeld, 2001), and *Bulimina* spp. can adapt well to a low oxygen and high sulfide cold seep environment, even in shallow waters (Panieri, 2006). The high density of this species related to methane seepage lead to another increase above the layer in which gas hydrate dissociated.

Triggering Mechanism for the Submarine Landslides in the Dongsha Area

Gravity flows such as submarine landslides and turbidity currents are ubiquitous in Dongsha area (Li et al., 2020). And these gravity flows are proved to be able to drive erosion and deposition in Taiwan submarine canyons. As shown on the bathymetric and seismic profiles close to the research areas. Recurrent MTDs are identified in the slope, which indicate Dongsha slope might be eroded by slope failures. And Li et al. (2020) concluded that a combined action of recurrent slope instability and turbidity currents drive the erosion and deposition of submarine asymmetry in our studying area. But from the C-M plot (**Figure 6**) (Passega, 1964), a common method to identify the force of deposition using the sediment size. The grain size distribution in the 4.4–6.0 m bsf layer in core 973-4 is not parallel to the RQ line in the, which indicated that sedimentation was not impacted by turbidity currents. Thus we contribute the gravity flows recorded in our sediment cores to submarine landslides.

The sediment particle size results in the three cores, 973-3 (Chen et al., 2014), 973-4 and 973-5, which were located at the top, middle and bottom of the Dongsha area continental slope, were comprehensively investigated. The submarine landslides in this study area mainly developed at the top of the continental slope, with lower intensity in the middle slope, and only landslide deposits were present at the bottom of the slope. Furthermore, the age reversal interval (**Figure 2**) coincided with the high foraminifera and sand content in layer 4.4–6.0 m bsf in core 973-4, which is consistent with frequent submarine landslides influencing this area (Zhong et al., 2015; Lin et al., 2016; Wu et al., 2018).

Based on a comprehensive analysis of geochemical and sediment records, gas hydrate dissociation events and submarine landslides were recognized in two cores. We take 973-4 for analyzing (**Figure 7**). There was sustained and stable methane seepage during the beginning of MIS2 (6.0–9.0 m, **Figure 7A**) and the methane flux was relatively low. Therefore, iron sulfides with high $\delta^{34}S_{CRS}$ and benthic foraminifera with negative $\delta^{13}C$ were found in the sediment layer (**Figure 7A**). At the end of MIS2, responding to the LGM period (4.0–6.0 m), the methane flux was very high and the SMTZ was near the seafloor (**Figure 7B**). In this case, the enrichment of TOC might be due to the lower rates of AOM and higher methane flux into the water column (Consolaro et al., 2015). More importantly, the massive decomposition of gas hydrate during the low-stand sea level period reduced slope stability (Sultan et al., 2010; Kwon et al., 2011), and herein led to the formation of the submarine landslides and sediment transportation from the top to the flat area of the slope (**Figure 7B**). The abrupt increase in benthic foraminifera quantity also verify this geological activity. Because methane diffused into the atmosphere before it had completely reacted, the $\delta^{34}S_{CRS}$ values of iron sulfides were low but the $\delta^{13}C$ values of benthic foraminifera showed negative anomalies (**Figure 7B**). Since the Last Glacial period (above 4.0 m), rising sea level has prevented the decomposition of gas hydrates and gradually

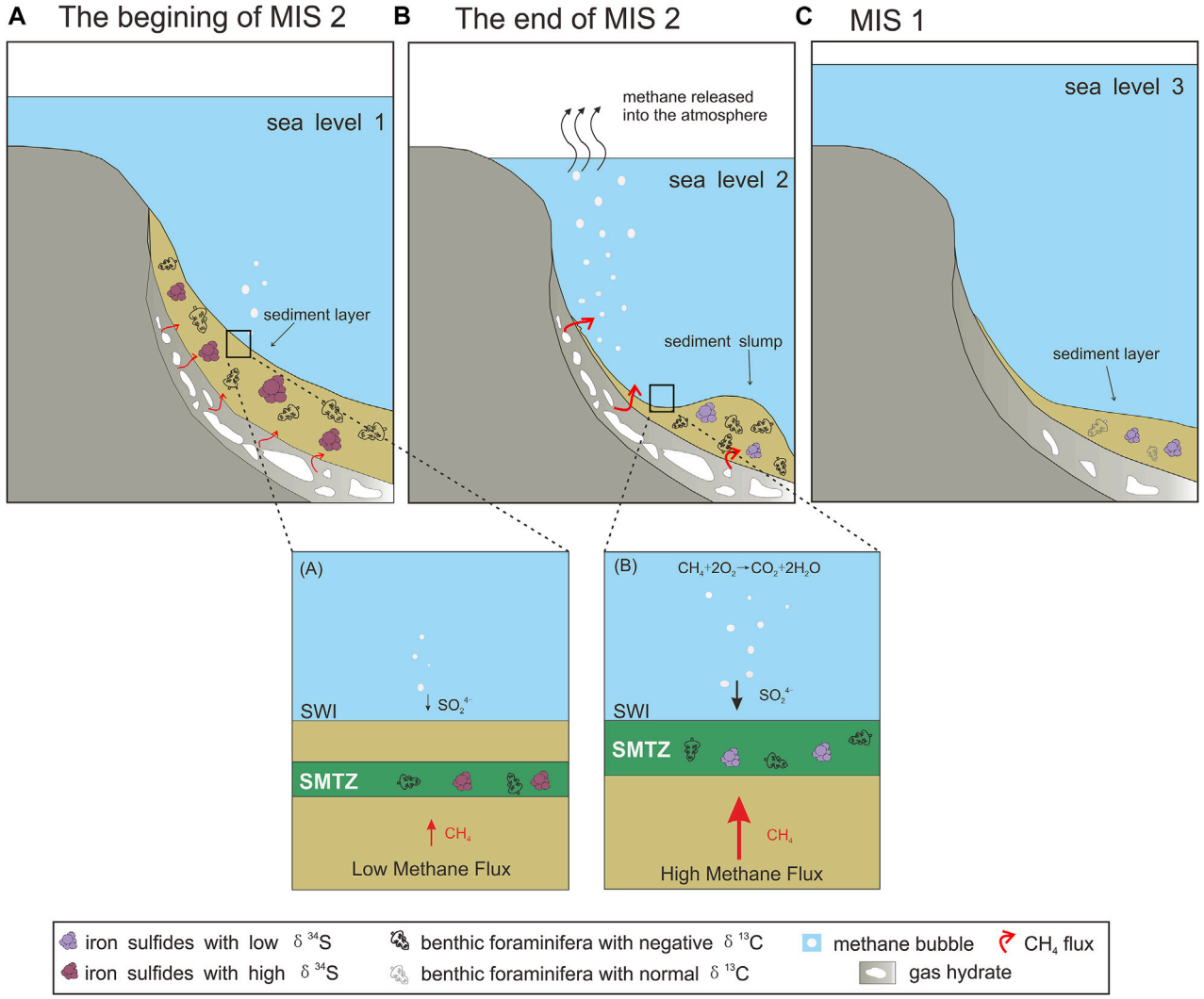

FIGURE 7 | Relationship between gas hydrate decomposition and submarine landslides (SWI: sea water interface).

weakened cold seep activity. Thus, the geochemical and benthic foraminifera records showed no further anomalies (**Figure 7C**).

CONCLUSION

Two sediment cores from the Dongsha slope in the SCS were used to identify gas hydrate dissociation events and subsequently the potential trigger of submarine landslides. The distinctly negative $\delta^{13}C$ values and positive $\delta^{18}O$ values along with extremely positive $\delta^{34}S_{CRS}$ values in both cores at the end of the LGM period suggested that there were persistent gas hydrate dissociation events in the Dongsha area during this period. In core 973-4, obvious submarine landslide deposits only occurred at the 4.4–6.0 m interval (end of LGM), and the numbers of *Uvigerina* spp. and *Bulimina* spp. sharply increased in this horizon. These results implied that the submarine landslides were probably caused by intense methane release events during this period. More importantly, as shown here, a novel strategy with geochemical methods were used to investigate the relationship between submarine landslides and gas hydrate dissociation events. Further studies of numerical methods are needed to quantitatively illustrate the casual relationship between them.

DATA AVAILABILITY STATEMENT

The raw data supporting the conclusion of this article will be made available by the authors, without undue reservation.

AUTHOR CONTRIBUTIONS

Formal analysis and writing—original draft preparation, YH; writing—review and editing, JC, MW, SW, and WY; All

authors have read and agreed to the published version of the manuscript.

FUNDING

Our work is supported by Key Special Project for Introduced Talents Team of Southern Marine Science and Engineering Guangdong Laboratory (Guangzhou) (GML2019ZD0104), the Innovation Development Fund of South China Sea Eco-Environmental Engineering Innovation Institute of the Chinese Academy of Sciences (ISEE2018PY02), the National Natural Science Foundation of China (41576035).

ACKNOWLEDGMENTS

We would like to thank all the crew members of the R/V Ocean VI of the 2011 Guangzhou Marine Geological Survey cruise. We acknowledge Dr. Peng for measuring sulfur isotopic compositions.

REFERENCES

Abu-Zied, R. H., Rohling, E. J., Jorissen, F. J., Fontanier, C., Casford, J. S. L., and Cooke, S. (2008). Benthic Foraminiferal Response to Changes in Bottom-Water Oxygenation and Organic Carbon Flux in the Eastern Mediterranean during LGM to Recent Times. *Mar. Micropaleontol.* 67 (1-2), 46–68. doi:10.1016/j.marmicro.2007.08.006

Aharon, P., and Fu, B. S. (2003). Sulfur and Oxygen Isotopes of Coeval Sulfate-Sulfide in Pore Fluids of Cold Seep Sediments with Sharp Redox Gradients. *Chem. Geol.* 195 (1-4), 201–218. doi:10.1016/s0009-2541(02)00395-9

Bayon, G., Henderson, G. M., Etoubleau, J., Caprais, J.-C., Ruffine, L., Marsset, T., et al. (2015). U-Th Isotope Constraints on Gas Hydrate and Pockmark Dynamics at the Niger Delta Margin. *Mar. Geol.* 370, 87–98. doi:10.1016/j.margeo.2015.10.012

Berner, R. A. (1982). Burial of Organic Carbon and Pyrite Sulfur in the Modern Ocean; its Geochemical and Environmental Significance. *Am. J. Sci.* 282 (4), 451–473. doi:10.2475/ajs.282.4.451

Boetius, A., Ravenschlag, K., Schubert, C. J., Rickert, D., Widdel, F., Gieseke, A., et al. (2000). A Marine Microbial Consortium Apparently Mediating Anaerobic Oxidation of Methane. *Nature* 407 (6804), 623–626. doi:10.1038/35036572

Boetius, A., and Wenzhöfer, F. (2013). Seafloor Oxygen Consumption Fuelled by Methane from Cold Seeps. *Nat. Geosci.* 6 (9), 725–734. doi:10.1038/ngeo1926

Borowski, W. S., Rodriguez, N. M., Paull, C. K., and Ussler, W. (2013). Are 34S-Enriched Authigenic Sulfide Minerals a Proxy for Elevated Methane Flux and Gas Hydrates in the Geologic Record? *Mar. Petroleum Geol.* 43, 381–395. doi:10.1016/j.marpetgeo.2012.12.009

Canfield, D. E., Raiswell, R., Westrich, J. T., Reaves, C. M., and Berner, R. A. (1986). The Use of Chromium Reduction in the Analysis of Reduced Inorganic Sulfur in Sediments and Shales. *Chem. Geol.* 54 (1-2), 149–155. doi:10.1016/0009-2541(86)90078-1

Canfield, D. E., and Thamdrup, B. (1994). The Production of 34 S-Depleted Sulfide during Bacterial Disproportionation of Elemental Sulfur. *Science* 266 (5193), 1973–1975. doi:10.1126/science.11540246

Chaytor, J. D., ten Brink, U. S., Solow, A. R., and Andrews, B. D. (2009). Size Distribution of Submarine Landslides along the US Atlantic Margin. *Mar. Geol.* 264 (1-2), 16–27. doi:10.1016/j.margeo.2008.08.007

Chen, D. F., Huang, Y. Y., Yuan, X. L., and Cathles, L. M. (2005). Seep Carbonates and Preserved Methane Oxidizing Archaea and Sulfate Reducing Bacteria Fossils Suggest Recent Gas Venting on the Seafloor in the Northeastern South China Sea. *Mar. Petroleum Geol.* 22 (5), 613–621. doi:10.1016/j.marpetgeo.2005.05.002

Chen, F., Hu, Y., Feng, D., Zhang, X., Cheng, S., Cao, J., et al. (2016). Evidence of Intense Methane Seepages from Molybdenum Enrichments in Gas Hydrate-Bearing Sediments of the Northern South China Sea. *Chem. Geol.* 443, 173–181. doi:10.1016/j.chemgeo.2016.09.029

Chen, F., Wang, X., Li, N., Cao, G., and Peckmann, J. (2019). Gas Hydrate Dissociation during Sea-Level Highstand Inferred from U/Th Dating of Seep Carbonate from the South China Sea. *Geophys. Res. Lett.* 46, 13928–13938. doi:10.1029/2019GL085643

Chen, F., Xin, S. U., Hongfeng, L. U., Chaoyun, C., Yang, Z., Sihai, C., et al. (2007). Carbon Stable Isotopic Composition of Benthic Foraminifers from the Northern of the South China Sea: Indicator of Methane-Rich Environment. *Mar. Geol. Quat. Geol.* 27 (4), 1–7.

Chen, F., Zhuang, C., Zhang, G., Lu, H., Duan, X., Zhou, Y., et al. (2014). Abnormal Sedimentary Events and Gas Hydrate Dissociation in Dongsha Area of the South China Sea during Last Glacial Period. *Earth Sci.-J. China U. Geosci.* 39 (11), 1517–1526. doi:10.3799/dqkx.2014.144

Colin, F., Ker, S., Riboulot, V., and Sultan, N. (2020). Irregular BSR: Evidence of an Ongoing Reequilibrium of a Gas Hydrate System. *Geophys. Res. Lett.* 47, 20. doi:10.1029/2020GL089906

Consolaro, C., Rasmussen, T. L., Panieri, G., Mienert, J., Bünz, S., and Sztybor, K. (2015). Carbon Isotope (δ¹³C) Excursions Suggest Times of Major Methane Release during the Last 14 Kyr in Fram Strait, the Deep-Water Gateway to the Arctic. *Clim. Past.* 11 (4), 669–685. doi:10.5194/cp-11-669-2015

Eiger, J., Berndt, C., Krastel, S., Piper, D. J. W., Gross, F., and Geissler, W. H. (2017). Chronology of the Fram Slide Complex Offshore NW Svalbard and its Implications for Local and Regional Slope Stability. *Mar. Geol.* 393, 141–155. doi:10.1016/j.margeo.2016.11.003

Feng, D., and Chen, D. (2015). Authigenic Carbonates from an Active Cold Seep of the Northern South China Sea: New Insights into Fluid Sources and Past Seepage Activity. *Deep Sea Res. Part II Top. Stud. Oceanogr.* 122, 74–83. doi:10.1016/j.dsr2.2015.02.003

Fontanier, C., Mackensen, A., Jorissen, F. J., Anschutz, P., Licari, L., and Griveaud, C. (2006). Stable Oxygen and Carbon Isotopes of Live Benthic Foraminifera from the Bay of Biscay: Microhabitat Impact and Seasonal Variability. *Mar. Micropaleontol.* 58 (3), 159–183. doi:10.1016/j.marmicro.2005.09.004

Formolo, M. J., and Lyons, T. W. (2013). Sulfur Biogeochemistry of Cold Seeps in the Green Canyon Region of the Gulf of Mexico. *Geochimica Cosmochimica Acta* 119, 264–285. doi:10.1016/j.gca.2013.05.017

Gong, S., Hu, Y., Li, N., Feng, D., Liang, Q., Tong, H., et al. (2018). Environmental Controls on Sulfur Isotopic Compositions of Sulfide Minerals in Seep Carbonates from the South China Sea. *J. Asian Earth Sci.* 168, 96–105. doi:10.1016/j.jseaes.2018.04.037

Han, X., Suess, E., Liebetrau, V., Eisenhauer, A., and Huang, Y. (2014). Past Methane Release Events and Environmental Conditions at the Upper Continental Slope of the South China Sea: Constraints by Seep Carbonates. *Int. J. Earth Sci. Geol. Rundsch* 103 (7), 1873–1887. doi:10.1007/s00531-014-1018-5

Handwerger, A. L., Rempel, A. W., and Skarbek, R. M. (2017). Submarine Landslides Triggered by Destabilization of High-Saturation Hydrate Anomalies. *Geochem. Geophys. Geosyst.* 18 (7), 2429–2445. doi:10.1002/2016gc006706

Herguera, J. C., Paull, C. K., Perez, E., Ussler, W., III, and Peltzer, E. (2014). Limits to the Sensitivity of Living Benthic Foraminifera to Pore Water Carbon Isotope Anomalies in Methane Vent Environments. *Paleoceanography* 29 (3), 273–289. doi:10.1002/2013pa002457

Horozal, S., Bahk, J.-J., Urgeles, R., Kim, G. Y., Cukur, D., Kim, S.-P., et al. (2017). Mapping Gas Hydrate and Fluid Flow Indicators and Modeling Gas Hydrate Stability Zone (GHSZ) in the Ulleung Basin, East (Japan) Sea: Potential Linkage between the Occurrence of Mass Failures and Gas Hydrate Dissociation. *Mar. Petroleum Geol.* 80, 171–191. doi:10.1016/j.marpetgeo.2016.12.001

Hu, Y., Chen, L., Feng, D., Liang, Q., Xia, Z., and Chen, D. (2017). Geochemical Record of Methane Seepage in Authigenic Carbonates and Surrounding Host Sediments: A Case Study from the South China Sea. *J. Asian Earth Sci.* 138, 51–61. doi:10.1016/j.jseaes.2017.02.004

Jorgensen, B. B., Bottcher, M. E., Luschen, H., Neretin, L. N., and Volkov, I., II (2004). Anaerobic Methane Oxidation and a Deep H2S Sink Generate Isotopically Heavy Sulfides in Black Sea Sediments. *Geochim. Cosmochim. Ac.* 68 (9), 2095–2118. doi:10.1016/j.gca.2003.07.017

Kaneko, M., Shingai, H., Pohlman, J. W., and Naraoka, H. (2010). Chemical and Isotopic Signature of Bulk Organic Matter and Hydrocarbon Biomarkers within Mid-slope Accretionary Sediments of the Northern Cascadia Margin Gas Hydrate System. *Mar. Geol.* 275 (1-4), 166–177. doi:10.1016/j.margeo.2010.05.010

Karstens, J., Haflidason, H., Becker, L. W. M., Berndt, C., Rüpke, L., Planke, S., et al. (2018). Glacigenic Sedimentation Pulses Triggered Post-glacial Gas Hydrate Dissociation. *Nat. Commun.* 9, 635. doi:10.1038/s41467-018-03043-z

Kayen, R. E., and Lee, H. J. (1991). Pleistocene Slope Instability of Gas Hydrate-Laden Sediment on the Beaufort Sea Margin. *Mar. Geotec.* 10 (1-2), 125–141. doi:10.1080/10641199109379886

Kwon, T.-H., Lee, K.-R., Cho, G.-C., and Lee, J. Y. (2011). Geotechnical Properties of Deep Oceanic Sediments Recovered from the Hydrate Occurrence Regions in the Ulleung Basin, East Sea, Offshore Korea. *Mar. Petroleum Geol.* 28 (10), 1870–1883. doi:10.1016/j.marpetgeo.2011.02.003

Leynaud, D., Mienert, J., and Nadim, F. (2004). Slope Stability Assessment of the Helland Hansen Area Offshore the Mid-Norwegian Margin. *Mar. Geol.* 213 (1-4), 457–480. doi:10.1016/j.margeo.2004.10.019

Li, G., Moridis, G. J., Zhang, K., and Li, X.-S. (2011). The Use of Huff and Puff Method in a Single Horizontal Well in Gas Production from Marine Gas Hydrate Deposits in the Shenhu Area of South China Sea. *J. Petroleum Sci. Eng.* 77 (1), 49–68. doi:10.1016/j.petrol.2011.02.009

Li, N., Yang, X., Peng, J., Zhou, Q., and Chen, D. (2018). Paleo-cold Seep Activity in the Southern South China Sea: Evidence from the Geochemical and Geophysical Records of Sediments. *J. Asian Earth Sci.* 168, 106–111. doi:10.1016/j.jseaes.2017.10.022

Li, W., Li, S., Alves, T. M., Rebesco, M., and Feng, Y. (2021). The Role of Sediment Gravity Flows on The Morphological Development of A Large Submarine Canyon (Taiwan Canyon), North-East South China Sea. *Sedimentology* 68, 1091–1108. doi:10.1111/sed.12818

Lim, Y. C., Lin, S., Yang, T. F., Chen, Y.-G., and Liu, C.-S. (2011). Variations of Methane Induced Pyrite Formation in the Accretionary Wedge Sediments Offshore Southwestern Taiwan. *Mar. Petroleum Geol.* 28 (10), 1829–1837. doi:10.1016/j.marpetgeo.2011.04.004

Lin, Q., Wang, J., Taladay, K., Lu, H., Hu, G., Sun, F., et al. (2016). Coupled Pyrite Concentration and Sulfur Isotopic Insight into the Paleo Sulfate-Methane Transition Zone (SMTZ) in the Northern South China Sea. *J. Asian Earth Sci.* 115, 547–556. doi:10.1016/j.jseaes.2015.11.001

Liu, J., Izon, G., Wang, J., Antler, G., Wang, Z., Zhao, J., et al. (2018). Vivianite Formation in Methane-Rich Deep-Sea Sediments from the South China Sea. *Biogeo. Discuss.* 15, 6329–6348. doi:10.5194/bg-15-6329-2018

Panieri, G. (2005). Benthic Foraminifera Associated with a Hydrocarbon Seep in the Rockall Trough (NE Atlantic). *Geobios* 38 (2), 247–255. doi:10.1016/j.geobios.2003.10.004

Panieri, G., Camerlenghi, A., Conti, S., Pini, G. A., and Cacho, I. (2009). Methane Seepages Recorded in Benthic Foraminifera from Miocene Seep Carbonates, Northern Apennines (Italy). *Palaeogeogr. Palaeocl.* 284 (3-4), 271–282. doi:10.1016/j.palaeo.2009.10.006

Panieri, G. (2006). Foraminiferal Response to an Active Methane Seep Environment: A Case Study from the Adriatic Sea. *Mar. Micropaleontol.* 61 (1-3), 116–130. doi:10.1016/j.marmicro.2006.05.008

Panieri, G., Lepland, A., Whitehouse, M. J., Wirth, R., Raanes, M. P., James, R. H., et al. (2017). Diagenetic Mg-Calcite Overgrowths on Foraminiferal Tests in the Vicinity of Methane Seeps. *Earth Planet. Sci. Lett.* 458, 203–212. doi:10.1016/j.epsl.2016.10.024

Passega, R. (1964). Grain Size Representation by CM Patterns as a Geologic Tool. *J. Sediment. Res.* 34 (4), 830–847. doi:10.1306/74d711a4-2b21-11d7-8648000102c1865d

Peckmann, J., and Thiel, V. (2004). Carbon Cycling at Ancient Methane-Seeps. *Chem. Geol.* 205 (3-4), 443–467. doi:10.1016/j.chemgeo.2003.12.025

Peketi, A., Mazumdar, A., Joshi, R. K., Patil, D. J., Srinivas, P. L., and Dayal, A. M. (2012). Tracing the Paleo Sulfate-Methane Transition Zones and H2S Seepage Events in Marine Sediments: An Application of C-S-Mo Systematics. *Geochem. Geophy. Geosy.* 13 (10), 1–11. doi:10.1029/2012gc004288

Pierre, C., Blanc-Valleron, M.-M., Caquineau, S., März, C., Ravelo, A. C., Takahashi, K., et al. (2016). Mineralogical, Geochemical and Isotopic Characterization of Authigenic Carbonates from the Methane-Bearing Sediments of the Bering Sea Continental Margin (IODP Expedition 323, Sites U1343-U1345). *Deep Sea Res. Part II Top. Stud. Oceanogr.* 125-126, 133–144. doi:10.1016/j.dsr2.2014.03.011

Portilho-Ramos, R. C., Cruz, A. P. S., Barbosa, C. F., Rathburn, A. E., Mulitza, S., Venancio, I. M., et al. (2018). Methane Release from the Southern Brazilian Margin during the Last Glacial. *Sci. Rep.* 8, 5948. doi:10.1038/s41598-018-24420-0

Rathburn, A. E., Levin, L. A., Held, Z., and Lohmann, K. C. (2000). Benthic Foraminifera Associated with Cold Methane Seeps on the Northern California Margin: Ecology and Stable Isotopic Composition. *Mar. Micropaleontol.* 38 (3-4), 247–266. doi:10.1016/s0377-8398(00)00005-0

Rathburn, A. E., Perez, M. E., Martin, J. B., Day, S. A., Mahn, C., Gieskes, J., et al. (2003). Relationships between the Distribution and Stable Isotopic Composition of Living Benthic Foraminifera and Cold Methane Seep Biogeochemistry in Monterey Bay, California. *Geochem. Geophy. Geosy.* 4, 1106. doi:10.1029/2003gc000595

Roberts, H. H., and Aharon, P. (1994). Hydrocarbon-derived Carbonate Buildups of the Northern Gulf-Of- Mexico Continental Slope- a Review of Submersible Investigations. *Geo-Mar. Lett.* 14 (2-3), 135–148. doi:10.1007/bf01203725

Sato, H., Hayashi, K.-I., Ogawa, Y., and Kawamura, K. (2012). Geochemistry of Deep Sea Sediments at Cold Seep Sites in the Nankai Trough: Insights into the Effect of Anaerobic Oxidation of Methane. *Mar. Geol.* 323-325, 47–55. doi:10.1016/j.margeo.2012.07.013

Schmiedl, G., Pfeilsticker, M., Hemleben, C., and Mackensen, A. (2004). Environmental and Biological Effects on the Stable Isotope Composition of Recent Deep-Sea Benthic Foraminifera, from the Western Mediterranean Sea. *Mar. Micropaleontol.* 51 (1-2), 129–152. doi:10.1016/j.marmicro.2003.10.001

Schneider, A., Crémière, A., Panieri, G., Lepland, A., and Knies, J. (2017). Diagenetic Alteration of Benthic Foraminifera from a Methane Seep Site on Vestnesa Ridge (NW Svalbard). *Deep Sea Res. Part I Oceanogr. Res. Pap.* 123, 22–34. doi:10.1016/j.dsr.2017.03.001

Schneider, A., Panieri, G., Lepland, A., Consolaro, C., Crémière, A., Forwick, M., et al. (2018). Methane Seepage at Vestnesa Ridge (NW Svalbard) since the Last Glacial Maximum. *Quat. Sci. Rev.* 193, 98–117. doi:10.1016/j.quascirev.2018.06.006

Schonfeld, J. (2001). Benthic Foraminifera and Pore-Water Oxygen Profiles: A Re-assessment of Species Boundary Conditions at the Western Iberian Margin. *J. Foraminifer. Res.* 31 (2), 86–107. doi:10.2113/0310086

Screaton, E. J., Torres, M. E., Dugan, B., Heeschen, K. U., Mountjoy, J. J., Ayres, C., et al. (2019). Sedimentation Controls on Methane-Hydrate Dynamics Across Glacial/Interglacial Stages: An Example From International Ocean Discovery Program Site U1517, Hikurangi Margin. *Geochem. Geophys. Geosyst.* 20, 4906–4921. doi:10.1029/2019GC008603

Solheim, A., Berg, K., Forsberg, C. F., and Bryn, P. (2005). The Storegga Slide Complex: Repetitive Large Scale Sliding with Similar Cause and Development. *Mar. Pet. Geol.* 22 (1-2), 97–107. doi:10.1016/b978-0-08-044694-3.50012-3

Stott, L. D., Bunn, T., Prokopenko, M., Mahn, C., Gieskes, J., and Bernhard, J. M. (2002). Does the Oxidation of Methane Leave an Isotopic Fingerprint in the Geologic Record? *Geochem. Geophy. Geosy.* 3 (2), 1–16. doi:10.1029/2001gc000196

Su, Z., He, Y., Wu, N., Zhang, K., and Moridis, G. J. (2012). Evaluation on Gas Production Potential from Laminar Hydrate Deposits in Shenhu Area of South China Sea through Depressurization Using Vertical Wells. *J. Petroleum Sci. Eng.* 86-87, 87–98. doi:10.1016/j.petrol.2012.03.008

Sultan, N., Marsset, B., Ker, S., Marsset, T., Voisset, M., Vernant, A. M., et al. (2010). Hydrate Dissolution as a Potential Mechanism for Pockmark Formation in the Niger Delta. *J. Geophys. Res.* 115, 1–33. doi:10.1029/2010jb007453

Tong, H., Feng, D., Cheng, H., Yang, S., Wang, H., Min, A. G., et al. (2013). Authigenic Carbonates from Seeps on the Northern Continental Slope of the

South China Sea: New Insights into Fluid Sources and Geochronology. *Mar. Petroleum Geol.* 43, 260–271. doi:10.1016/j.marpetgeo.2013.01.011

Uchida, M., Shibata, Y., Ohkushi, K., Ahagon, N., and Hoshiba, M. (2004). Episodic Methane Release Events from Last Glacial Marginal Sediments in the Western North Pacific. *Geochem. Geophy. Geosy* 5 (8), 1–14. doi:10.1029/2004gc000699

Wang, C. (2013). *The Magnetic Parameters and its Environmental Implications in Sediments since Late Pleistocene from Dongsha Area, South China Sea*. Beijing: China University of Geosciences, 1–45.

Wefer, G., Heinze, P.-M., and Berger, W. H. (1994). Clues to Ancient Methane Release. *Nature* 369 (6478), 282. doi:10.1038/369282a0

Wei, G.-J., Huang, C.-Y., Wang, C.-C., Lee, M.-Y., and Wei, K.-Y. (2006). High-resolution Benthic Foraminifer Delta C-13 Records in the South China Sea during the Last 150 Ka. *Mar. Geol.* 232 (3-4), 227–235. doi:10.1016/j.margeo.2006.08.005

Wu, X., Liang, Q., Ma, Y., Shi, Y., Xia, Z., Liu, L., et al. (2018). Submarine Landslides and Their Distribution in the Gas Hydrate Area on the North Slope of the South China Sea. *Energies* 11, 3481. doi:10.3390/en11123481

Yan, P., Deng, H., and Liu, H. (2006). The Geological Structure and Prospect of Gas Hydrate over the Dongsha Slope, South China Sea. *Terr. Atmos. Ocean. Sci.* 17 (4), 645–658. doi:10.3319/tao.2006.17.4.645(gh)

Yu, X., Wang, J., Li, S., Fang, J., Jiang, L., Cong, X., et al. (2013). The Relationship between Tectonic Subsidence and BSR of Upper Neogene in the Deep-Water Area of the Northern Continental Slope, South China Sea. *Acta Geol. sin-engl.* 87 (3), 804–818.

Zhang, B., Pan, M., Wu, D., and Wu, N. (2018). Distribution and Isotopic Composition of Foraminifera at Cold-Seep Site 973-4 in the Dongsha Area, Northeastern South China Sea. *J. Aaian Earth Sci.* 168, 14–154. doi:10.1016/j.jseaes.2018.05.007

Zhong, G., Cartigny, M. J. B., Kuang, Z., and Wang, L. (2015). Cyclic Steps along the South Taiwan Shoal and West Penghu Submarine Canyons on the Northeastern Continental Slope of the South China Sea. Geol. Sos. *Am. Bull.* 127 (5-6), 804–824. doi:10.1130/b31003.1

Zhu, M.-X., Shi, X.-N., Yang, G.-P., and Hao, X.-C. (2013). Formation and Burial of Pyrite and Organic Sulfur in Mud Sediments of the East China Sea Inner Shelf: Constraints from Solid-phase Sulfur Speciation and Stable Sulfur Isotope. *Cont. Shelf Res.* 54, 24–36. doi:10.1016/j.csr.2013.01.002

Conflict of Interest: The authors declare that the research was conducted in the absence of any commercial or financial relationships that could be construed as a potential conflict of interest.

Publisher's Note: All claims expressed in this article are solely those of the authors and do not necessarily represent those of their affiliated organizations, or those of the publisher, the editors and the reviewers. Any product that may be evaluated in this article, or claim that may be made by its manufacturer, is not guaranteed or endorsed by the publisher.